Ocean Sci. Discuss., https://doi.org/10.5194/os-2018-83
Manuscript under review for journal Ocean Sci.
Discussion started: 6 September 2018

Ocean Science
Discussions
Open Access
EGU

The land-sea coastal border: A quantitative definition

Agustín Sánchez-Arcilla[1], Jue Lin-Ye[1], Manuel García-León[1], Vicente Gràcia[1], and Elena Pallarès[1,2]

[1]Laboratory of Maritime Engineering, Barcelona Tech, D1 Campus Nord, Jordi Girona 1-3, 08034, Barcelona, Spain
[2]EUSS - Escola Universitaria Salesiana de Sarria, Sant Joan Bosco 74, 08017, Barcelona, Spain

Correspondence: A. Sánchez-Arcilla (agustin.arcilla@upc.edu)

Abstract. A quantitative definition for the land-sea (coastal) transitional area is here proposed, based on variability and isotropy of met-ocean processes. Wind velocity and significant wave height fields are examined for anisotropy along four perpendicular transects on the Catalan coast (northwestern Mediterranean) illustrating a case of significant changes along shelf. The variation of anisotropy as a function of distance from the coast and water depth has been analyzed through heatmaps and scatter plots. The results show how the anisotropy of wind velocity and significant wave height decrease towards the offshore, suggesting an objective definition for the coastal fringe width. The more robust estimator turns out to be the distance at which the significant wave height anisotropy is equal to the 90^{th} quantile of variance within a $100\mathrm{km}$ distance from the coast. Such a definition, when applied to the Spanish Mediterranean coast, determines a fringe of width of 2-$4\mathrm{km}$. Regarding the probabilistic characterization, the inverse of wind velocity anisotropy can be fitted to a lognormal distribution function, while the significant wave height anisotropy can be fitted to a log-logistic distribution function. The joint probability structure of the two anisotropies can be best described by a Gaussian copula, where the dependence parameter denotes mild to moderate dependence between both anisotropies, reflecting a certain decoupling between wind velocity and significant wave height near the coast. This wind-wave dependence remains stronger in the central, bay-like part of the study area, where the wave field is being more actively generated by the overlaying wind. Such a pattern controls the spatial variation of the coastal fringe width.

1 Introduction

Land-sea border areas are narrow strips of water that display unique met-ocean dynamics due to a) non-linearity and sea bottom interactions (including bathymetric control) for the ocean (Sánchez-Arcilla et al., 2016a) and b) differential heat over land/sea and topographic control on winds (e.g. channeled winds and coastal jets) (Bolaños et al., 2007; Sánchez-Arcilla et al., 2008, 2014). This results in enhanced gradients that interact with very productive ecosystems and a large number of infrastructures and socio-economic uses related to tourism, fisheries/aquaculture or maritime transport (Carniel et al., 2017; Sánchez-Arcilla et al., 2016a; Sierra et al., 2017). However, the limits of this land-sea transition remain fuzzy and even somewhat subjective, depending on the type of process or application considered and with technical, economic and legal implications.

There is, thus, a need for a systematic and objective definition of the coastal fringe that considers underlying processes and that has general applicability allowing for the time/space dynamics of this fringe. This type of approach has been explored in the literature, where for instance Sánchez-Arcilla and Simpson (2002) reviewed a number of possibilities based on a dynamic balance of competing processes such as inertial effects, geostrophic steering, sea bed friction or water column stratification.

Ocean Sci. Discuss., https://doi.org/10.5194/os-2018-83
Manuscript under review for journal Ocean Sci.
Discussion started: 6 September 2018

Wright and Short (1984) proposed a definition for the active beach profile, based on beach state and an environmental parameter function of the active hydrodynamics and the sediment fall velocity. The recent advent of high resolution and short revisit time provided by the new Sentinel data (Ahsbahs et al., 2017; Sánchez-Arcilla et al., 2017) offer an alternative source of information for such a coastal zone definition although with some limitations since the data may start degrading at a few kilometres (order $10\mathrm{km}$) offshore from the coast (Cavaleri and Sclavo, 2006). Because of that it is necessary to use high resolution numerical simulations supported by in-situ data so that land-sea boundary effects are properly captured for the subsequent coastal definition that will be based on the inhomogeneity introduced by the presence of the land boundary.

Anisotropy in wind and wave fields (Swail et al., 1999) can be an useful indicator of spatial structure, affected by topo-bathymetric constraints that generate substantial gradients in met-ocean conditions. It is well known that anisotropy can be a measure to define directional variation e.g. for mineral configuration in rocks (Amadei, 1996), for propagation velocity in heterogeneous media (Crampin, 1984) or for seismic waves (Verdon et al., 2008). Similarly, topographic induced anisotropy affects coastal wind patterns that force wave and current fields (Soomere, 2003).

The aim of this paper is to analyse coastal anisotropy and from that propose a new quantitative and objective definition for the land-sea border that benefits from high-resolution (spatial and temporal) wind and wave fields (Abdalla et al., 2011) and from the underlying process-based knowledge. This definition can be useful to determine a set of criteria for numerical purposes (e.g. nesting coastal domains) but also for more practically oriented applications (e.g. offshore limit for outfall dispersion). The analysis is based on a set of high-resolution wind and wave fields in the latter case using a well-tested code such as SWAN (Pallarés et al., 2014; Zijlema, 2010; Roland and Ardhuin, 2014). The numerical results, pertaining to a micro-tidal environment to avoid any distortion of spatial patterns by tides, will be subject to inexpensive statistical methods to characterize spatial structures. Following this approach, the paper is structured as follows. Section 2 introduces the theoretical background. Section 3 describes the study area, while the methodology is presented in Section 4. Section 5 lists the main results, which are discussed in Section 6, followed by some conclusions in Section 7.

2 Theoretical background

Anisotropic data fields are easily convertible to isotropic ones through rotation and rescaling (Chorti and Hristopulos, 2008). Being u and v the axes of the two principal directions (see Fig. 1), being θ ($\theta \in [0, 2\pi)$) the rotation in respect the principal coordinate system and $R = \frac{u}{v}$ ($R \in [0, \infty)$) the ratio between the principal axes of anisotropy, the new axes of the two principal directions can be obtained as:

$$u^* = u\cos\theta + v\sin\theta \tag{1}$$

$$v^* = (-u\sin\theta + v\cos\theta)\, R. \tag{2}$$

From this definition, it is aparent that R can serve to quantify the anisotropy of a data field.

Ocean Sci. Discuss., https://doi.org/10.5194/os-2018-83
Manuscript under review for journal Ocean Sci.
Discussion started: 6 September 2018

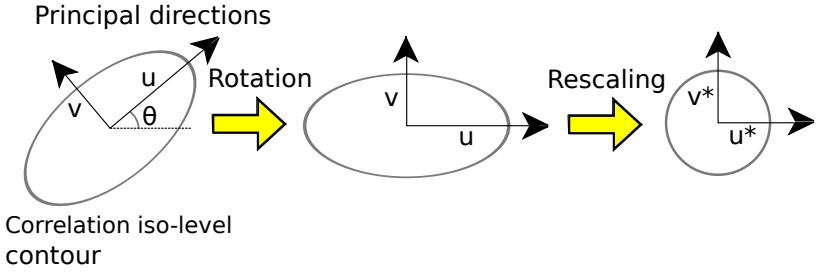

Figure 1. Transformation between anisotropic and isotropic fields. Supposing u and v are the two principal directions of anisotropy, any given anisotropic correlation iso-level contour can be converted into an isotropic one using the anisotropy ratio $R = \frac{u}{v} > 1$ and a certain rotation angle θ. The new field has a ratio $R^* = \frac{u^*}{v^*} = 1$.

Considering the ratio R as a variable for any 2D field, it can be fit to a probability distribution function. Such fitting depends on theoretical and practical considerations. The preferred shape is determined by looking at statistical characteristics such as mean, variance, skewness and kurtosis, or by examining the similarity between quantiles (dataset versus theoretical probability distribution) using a Quantile-Quantile plot. The more direct candidates to fit variable R are a) the log-normal function, where the probability distribution of its log-transform is Gaussian (Aitchison and Brown, 1957) and b) the log-logistic function, with a logistic probability distribution for the log-transformed variable. A logistic distribution has a probability density function of the form:

$$f(x) = \frac{1}{s} \exp\left((x-m)/s\right)\left(1+\exp\left((x-m)/s\right)\right)^{-2}, \tag{3}$$

where m is its location parameter and s is its scale parameter. Sklar's theorem (Sklar, 1959), expresses the multivariate joint probability structure of two variables x and y as the product of their cumulative probability distributions $F(x) = u$ and $G(x) = v$ (u and v here are not yet related to any definition of anisotropy), and a 2-D copula. The interval of variation of u, v is $[0,1]$ and a 2-D Gaussian copula has the form:

$$C_\rho(u,v) = \int_{-\infty}^{\Phi^{-1}(u)} \int_{-\infty}^{\Phi^{-1}(v)} \frac{1}{2\pi\sqrt{1-\rho_{12}^2}} \exp\left\{-\frac{s^2 - 2\rho_{12}st + t^2}{2(1-\rho_{12}^2)}\right\} \mathrm{d}s\mathrm{d}t. \tag{4}$$

where the correlation parameter $-1 < \rho_{12} < 1$ is used as the dependence parameter and Φ is the univariate standard normal distribution function (Embrechts et al., 2001). $\rho_{12} = 0$ means total independence between the variables, whereas $|\rho_{12}| = 1$ means total dependence. Whenever a joint probability structure has the form of a Gaussian copula, this structure can be applied without excessive computational cost (Li et al., 2014; Rueda et al., 2016), compared, for instance, to an Archimedean copula approach (Wahl et al., 2011; Lin-Ye et al., 2016; Okhrin et al., 2013).

Ocean Sci. Discuss., https://doi.org/10.5194/os-2018-83
Manuscript under review for journal Ocean Sci.
Discussion started: 6 September 2018

Ocean Science
Discussions
Open Access
EGU

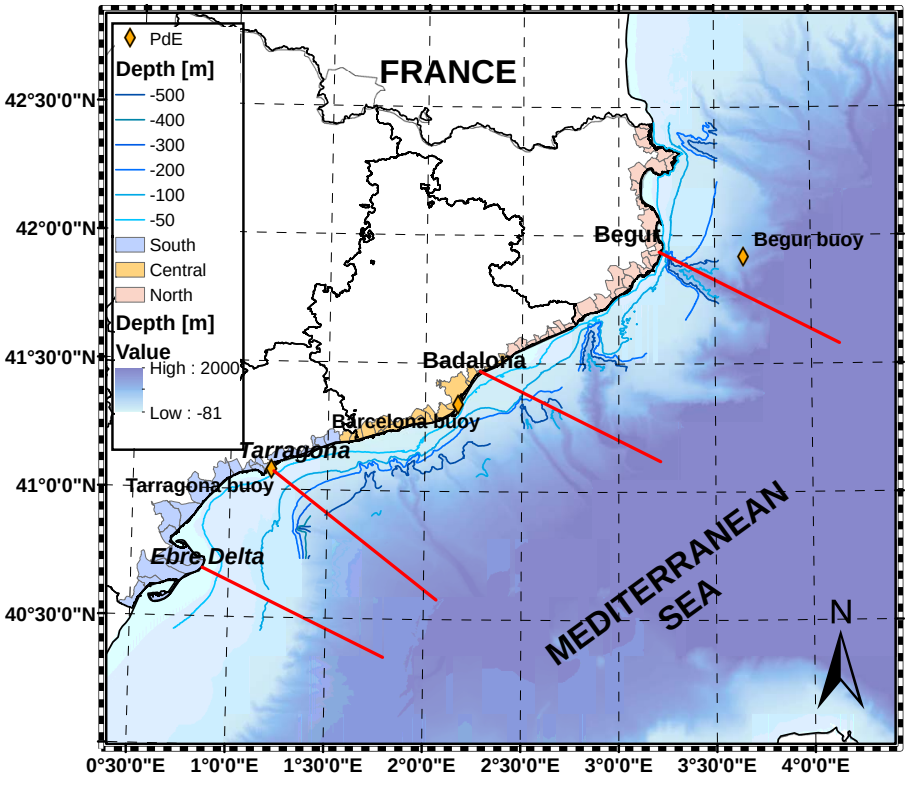

Figure 2. Study area, showing the gradients in topo-bathymetry that exert a strong control over the resulting met-ocean conditions. There are depicted the four transects (red lines) used to estimate the limit of the coastal fringe, located in a) Ebre Delta, b) Tarragona, c) Badalona and d) Begur. It also shows the Puertos del Estado (PdE) buoys and the division of the Catalan Coast into the northern, central and southern sections (different colours in the land part).

3 Study area

The selected pilot site for application is a micro-tidal environment such as the western Mediterranean Sea (Fig. 2), where enough validated met-ocean simulations exist and where the spatial wind/wave structure will not be distorted by tidal forcing. Current fields, slower to respond to the overlying meteorological driving, have not been considered in this initial analysis. The focus is on the Spanish north-eastern Mediterranean coast, where we have in-situ data available and Sentinel images for support. Moreover, the continental shelf varies in from 10km to more than 100km in an alongshore distance of less than 500km. The wind fields are affected (most frequent wind direction is from land, corresponding approximately to the north-west) by the presence of a mountain chain roughly parallel to the coastline and featuring several openings corresponding to river valleys. The anisotropy analysis has been performed at four characteristic transects, in terms of topo-bathymetric features. They correspond (Fig. 2) to the following locations (from south-west to north-east): Ebre (40.7°N, 0.87°E), Tarragona (41.12°N, 1.25°E), Mataro (41.53°N, 2.45°E) and Begur (42.28°N, 3.02°E).

Ocean Sci. Discuss., https://doi.org/10.5194/os-2018-83
Manuscript under review for journal Ocean Sci.
Discussion started: 6 September 2018

The north-western Mediterranean presents a particularly intense wind forcing (Jordi et al., 2011; Lebeaupin Brossier et al., 2012), which is shaped by local orography (Sierra et al., 2017). The Pyrenees mountain chain across the strip of land connecting the Iberian Peninsula to the European Continent forces a strong northern wind flux following the French-Spanish Mediterranean coast (Nicolle et al., 2009; Schaeffer et al., 2011; Obermann-Hellhund et al., 2017). This same wind pattern is channelled by the river valleys resulting in a north-western orientation for winds blowing from land to sea further down along the coast (Cerralbo et al., 2015), for latitudes southward of $41°N$. The most frequently observed patterns are, thus, from North in the coastal sector closer to the Pyrinees barrier and from the northwest further south, conditioned by the river valleys and gaps in the coastal parallel mountains (Bolaños and Sánchez-Arcilla, 2006; Lin-Ye et al., 2016; Obermann et al., 2016). The second most frequent pattern corresponds to western winds, associated to atmospheric depressions in northern Europe (Lin-Ye et al., 2017; Sánchez-Arcilla et al., 2014). Easterly winds are frequent during the summer, triggered by an intense high-pressure area over the British Islands.

The most common wave fields in the north-western Mediterranean Sea correspond to wind-sea (Bolaños et al., 2009; Sánchez-Arcilla et al., 2016b) forced by the easterly winds (Sánchez-Arcilla et al., 2008) and the northerly and north-westerly winds mentioned above. Because of the semi-enclosed character of the basin, the waves are fetch-limited (Bolaños and Sánchez-Arcilla, 2006), with maximum trajectory lengths around $600\mathrm{km}$, one-sixth of the average distance that a wave train travels across the Atlantic (García et al., 1993). The average wave-climate in the north-western Mediterranean Sea presents a mean significant wave height (H_s) of $0.78\mathrm{m}$ at the southern part of the Catalan coast, near the Ebre delta and slightly lower values (around $0.72\mathrm{m}$) further north and close to the French border. The spatial distribution for wave storms presents an opposite behaviour, with maximum H_s between $5.48\mathrm{m}$ in the southern sector and $5.85\mathrm{m}$ at the northern coastal stretch (Sánchez-Arcilla et al., 2008; Bolaños et al., 2009). Future projections Casas-Prat and Sierra (2013) indicate, for the interval 2071-2100 and A1B scenario (IPCC, 2000) a variation of the significant wave height around $\pm 10\%$, whereas the same variable for a 50year return-period exhibits rates of change around $\pm 20\%$.

4 Methods

The approach suggested for an objective assessment of anisotropy (leading to an automated definition of coastal boundaries) is schematized (Fig. 3). It requires high-resolution met-ocean fields to determine how the covariance of anisotropy evolves with distance to the land-sea border. The starting point are wind and associated wave fields, as the most promising candidates for reflecting the inhomogeneity induced by coastal topo-bathymetry. The wind fields have been provided by the UK-Met Office, from their Unified Model (Cullen, 1993) for weather and climate applications. This code solves the compressible, non-hydrostatic equations of motion with semi-Lagrangian advection and semi-implicit time stepping, including suitable parameterizations for sub-grid scale processes such as convection, boundary layer turbulence, radiation, cloud microphysics and orographic drag (Brown et al., 2012).

The computational domain covers the entire Mediterranean Sea using a regular grid with spacing of $\Delta\phi = 2.5°$ for latitude, of $\Delta\lambda = 3.75°$ for longitude and a time step of $1\mathrm{h}$. The associated wave fields have been calculated with the SWAN code,

Ocean Sci. Discuss., https://doi.org/10.5194/os-2018-83
Manuscript under review for journal Ocean Sci.
Discussion started: 6 September 2018

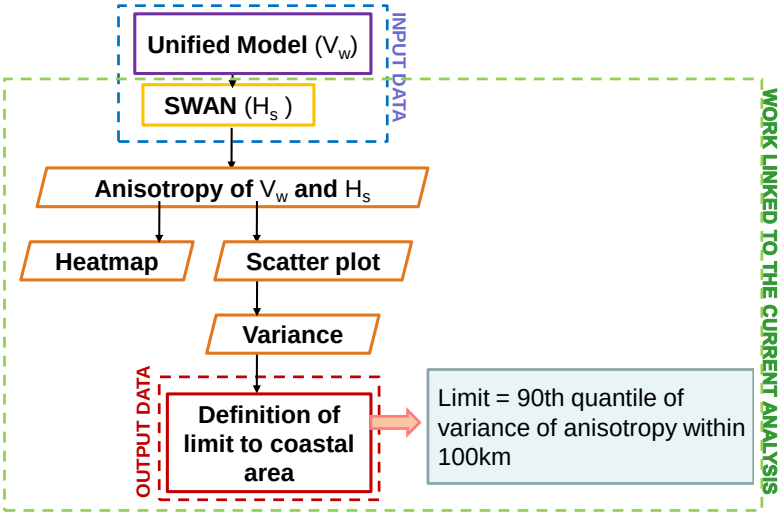

Figure 3. Flow-chart summarizing the methodology used in this paper. The dashed blue rectangle represents the input data, the red dashed rectangle indicates the output data and the green dashed rectangle shows the present analysis. Rectangles indicate data generation (input/output) and rhombuses the subsequent analyses of the proposed methodology.

covering the same geographical domain and with equal time step of 1h. SWAN is a spectral wave model based on the action balance equation (Booij et al., 1999) and including wave-wave interactions at various depths and whitecapping. It applies a fully implicit numerical scheme for propagation in geographical and spectral spaces that is unconditionally stable.

SWAN employs an unstructured grid with spatial resolutions of 600m-40km, higher near the land-sea boundary. Mesh sizes are determined objectively based on bathymetry gradients and distance to the coastline (Pallarés, 2016). Such a non-structured grid approach avoids nesting and internal boundary conditions, while maintaining a good spatial resolution to capture bottom and coastline irregularity (submarine canyons and capes or prodeltas that are found in the Catalan continental shelf). Furthermore, unstructured meshes are well suited to tackle non-linear effects (Chen et al., 2003; Jones and Davies, 2007; Lermusiaux et al., 2013). The resulting wave fields have been validated with two directional wave buoys at the northern and southern ends of the domain, managed by Puertos del Estado (Fig 2).

The independent variables used for analysing anisotropy are distance to the coast (x) and water depth (h). The anisotropy has been computed for the wind velocity at 10m over the mean sea-level (R_{V_w}) and for the significant wave height (R_{H_s}). R_{V_w} and R_{H_s} are taken to represent the behaviour of met-ocean conditions under the effect of the land-sea boundary (in this initial analysis height/depth gradients in topo-bathymetry). They have been calculated (1km spacing) along a 100km transect perpendicular to the coast (see Fig. 2), considering periods of 24h, long enough for the waves to respond to the acting wind forcing. Anisotropy needs to be computed on a regular grid and therefore, both wind velocity (V_w) and significant wave height (H_s) have been interpolated on a rectangular mesh. The interpolation method used in this case is the inverse distance weighted

Ocean Sci. Discuss., https://doi.org/10.5194/os-2018-83
Manuscript under review for journal Ocean Sci.
Discussion started: 6 September 2018

(IDW) interpolation, that estimates the value at an interpolated location (x) as the weighted average of neighbouring points with weights $w(x)$ given by

$$w(x) = \frac{1}{d(x, x_i)^p}. \tag{5}$$

Here, x_i is a neighbour point, d is the Euclidean distance and p is the inverse distance weighting power. The IDW power chosen is 1 for R_{V_w} and 3 for R_{H_s} and h, based on a sensitivity analysis for this area and consistent with the physical relation between wind velocity and generated wave height.

R (R_{V_w} or R_{H_s}) values are calculated for clusters of V_w or H_s within a circular sub-domain with radius of $5\mathrm{km}$. Heatmaps are used to represent the spatial distribution of anisotropy, showing how the density of R behaves as a function of distance to the coast and time (see Figs. 6 and 7). The elements selected to aggregate samples for the heatmap are hexagons with side $5\mathrm{km}$ and a scale for anisotropy of 20 units for both R_{V_w} and R_{H_s}. Both R and its variance are calculated on a discrete number of distances to the coastline, assuming that the width of the fringe affected by boundary effects is below $100\mathrm{km}$ for this coastal sector (Sánchez-Arcilla and Simpson, 2002). From here, it follows naturally to propose a coastal zone limit as the cutting point where the variance of R is equal to the 90^{th} quantile of the total R variance spanning a fringe between 0 and $100\mathrm{km}$:

$$l = 90^{th}\ quantile\ of\ \mathrm{var}\left(R_{H_s}\left(0\mathrm{km} \leq x \leq 100\mathrm{km}\right)\right) \tag{6}$$

This cutting point has shown, as expected, larger stability for the wave field than for the forcing wind patterns. The variation of R_{H_s} with coastal distance x (Fig. 7) indicates for reference the $20\mathrm{km}$ distance where satellite data offer enough robustness (Cavaleri and Sclavo, 2006). The plot also displays depth against x, after interpolation into a regular mesh (first on a grid of $1\mathrm{km}$, then to a finer mesh of $10\mathrm{m}$). The obtained R_{V_w} and R_{H_s} values have been fit to a probability distribution, selecting empirically the lognormal function for the inverse of R_{V_w} and the log-logistic function for R_{H_s}. The joint probability has been next adjusted to a Gaussian copula to capture the partial dependence structure.

5 Results

The SWAN model simulations have been validated with registered significant wave height (H_s) at the southern (Tarragona location) and northern (Begur location) coastal sectors (Figs. 4 and 5). The H_s buoy data show substantial coincidence with the simulated H_s, quantified in table 1 and in Figs. 4 and 5.

R_{V_w} and R_{H_s} have been analysed with heatmaps (Figs. 6 and 7) and scatterplots (Figs. 8 and 9). R_{V_w} presents values that span the interval from 1 to 250 and display a dependence on coastal distance (Fig. 6), featuring a combination of anisotropy close to the land boundary (0 to $20\mathrm{km}$) and then more isotropic behaviour towards the offshore (up to $100\mathrm{km}$), although with a rich variability. The wind fields present, in summary, a decreasing variance from 0 to $100\mathrm{km}$ with a pronounced slope from 0 to about $40\mathrm{km}$ (southern sector) or even further offshore (northern sector) and then an almost asymptotical trend. R_{H_s} behaves

Ocean Sci. Discuss., https://doi.org/10.5194/os-2018-83
Manuscript under review for journal Ocean Sci.
Discussion started: 6 September 2018

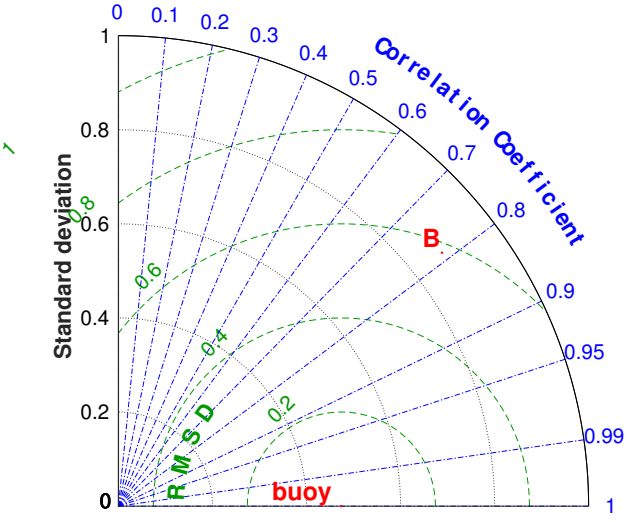

[a]

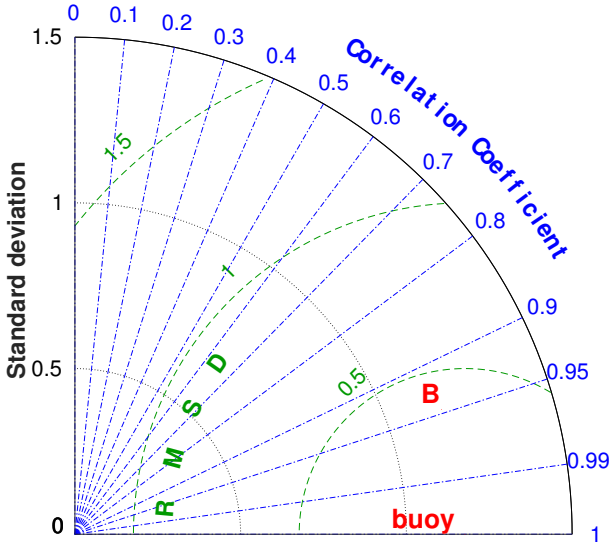

[b]

Figure 4. Taylor diagram showing correlation, standard deviation and root mean square error (R.M.S.E.) between numerical and observed data for a) south sector (Tarragona location) and b) north sector (Begur location), for the period November of 2016 to March of 2017.

Ocean Sci. Discuss., https://doi.org/10.5194/os-2018-83
Manuscript under review for journal Ocean Sci.
Discussion started: 6 September 2018

Ocean Science
Discussions
Open Access
EGU

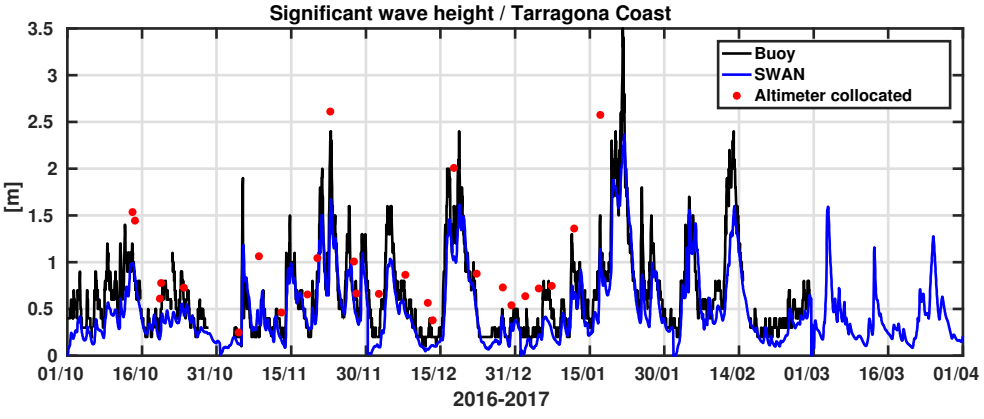

[a]

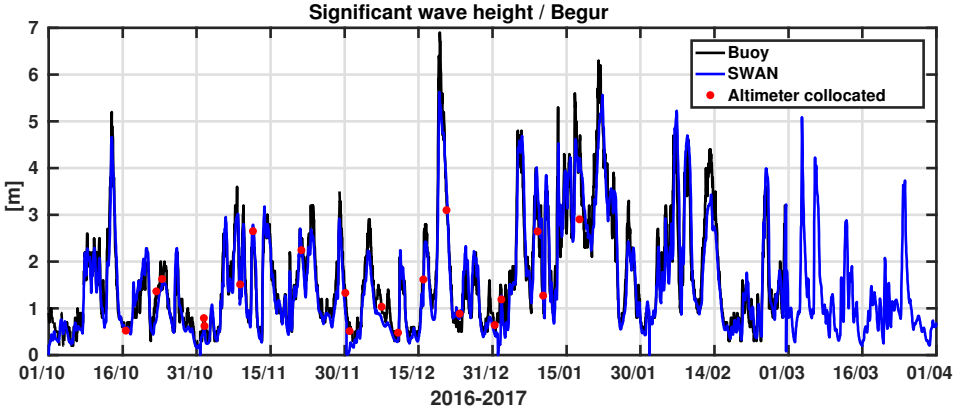

[b]

Figure 5. Comparison of numerically simulated significant wave height (SWAN model) with observations, for a) south sector (Tarragona location) and b) north sector (Begur location), for the period November of 2016 to March of 2017.

Table 1. Statistics of the agreement between numerical significant wave height fields (SWAN model) and observations in terms of root mean square error (R.M.S.E.), bias and scatter index (S.I.) for the control points at the southern and northern coastal sectors.

Buoy	R.M.S.E. [m]	bias [m]	S.I. [%]
Tarragona coastal buoy	0.248	−0.132	0.502
Begur	0.393	−0.087	0.249

similarly to R_{V_w}, but with a turning point at about $40\mathrm{km}$ in all transects (Figs. 8 and 9) and, thus, a higher level of consistency. The limit l, corresponding to the 90^{th} quantile of the total variance (fringe between 0 and $100\mathrm{km}$), is calculated from equation 6 (Figs. 8 and 9) and presents small differences with time interval (month of study) and location (sector), below the $1\mathrm{km}$ limit.

Ocean Sci. Discuss., https://doi.org/10.5194/os-2018-83
Manuscript under review for journal Ocean Sci.
Discussion started: 6 September 2018

In order to find a copula structure, marginal probability distributions for the two anisotropies are needed. Skewness and kurtosis from the analysed data show that the inverse anisotropy of V_w follows a log-normal distribution, while the anisotropy of H_s follows a log-logit distribution. Quantile-quantile plots have been used to assess the fit of each probability function (not shown here) to its target dataset, verifying that the selected samples can be adjusted to the corresponding probability distributions. The joint probability structure of the two anisotropies does not present any marked dependence for the largest (tail) values, suggesting the use of a Gaussian copula whose dependence parameter ρ is shown in Fig. 10. The so obtained dependence ranges from total independence (0) to a mild ($|\rho_{12}| = 0.1$) dependence between R_{V_w} and R_{H_s}.

6 Discussion

The calculated anisotropies should be as robust as the starting wave or wind fields that are employed in the analysis. Because of that, the SWAN code has been calibrated with local atmospheric and hydrodynamic conditions. Special emphasis has been put on using high quality wind fields, both for the direct assessment linked to meteo fields and for the indirect effect they exert on the behaviour of the forced hydrodynamics. The results show, as expected, a higher level of robustness for the wave-based anisotropy, where the calculations used an unstructured grid and a locally adjusted whitecapping term calibration (Pallarés et al., 2013, 2014). The cell size has been determined as a function of depth and distance to the coast (Pallarés, 2016), consistently with the transect analyses performed in the paper. The application of an unstructured grid allows reducing computational costs (by about 50%) and the troublesome imposition of internal boundaries, which facilitates multiple simulations to perform a statistically stable analysis of anisotropy. This leads to an efficient determination of the coastal water boundary that automatically incorporates some of the processes (e.g. turbulence levels in the water column due to wave action) and geometric settings (e.g. bathymetric gradients affecting wave fields). Other processes, such as for instance the continental discharge, are of course not captured by the present analysis and would require a similar approach based on the resulting circulation fields, which would certainly capture the regions of fresh-water influence.

The anisotropy-based approach will lead to different results depending on met-ocean conditions (wave conditions in our case), requiring a reliable simulation of both average and extreme patterns, as shown by the validation process (see e.g. Figs. 4 and 5). The transfer of energy from the coastal to the offshore domain and vice-versa (Pallarés et al., 2017) may condition the results of the analysis for areas near the transition, which is where the boundary will be likely located. This suggests a combined approach, using numerical fields and satellite data supplemented by along-track in situ observations, all suitably interpolated in space and time to provide a picture that is as consistent as possible.

The values of V_w, H_s and h obtained through the IDW interpolation, using an IDW weighting from 1 to 3, are similar and reasonable. For marine variables the weight of 3 has been selected, to account for the influence of the closest neighbours based on the water inertia (which is 3 orders of magnitude larger than for air). The proposed IDW power for V_w is smaller because gas is more turbulent than water and thus should have a smaller spatial dependence. The obtained pattern for R_{V_w} is consistent for the four selected transects in the study area, showing a mostly isotropic behaviour for coastal distances from 0 to 100km.

Ocean Sci. Discuss., https://doi.org/10.5194/os-2018-83
Manuscript under review for journal Ocean Sci.
Discussion started: 6 September 2018

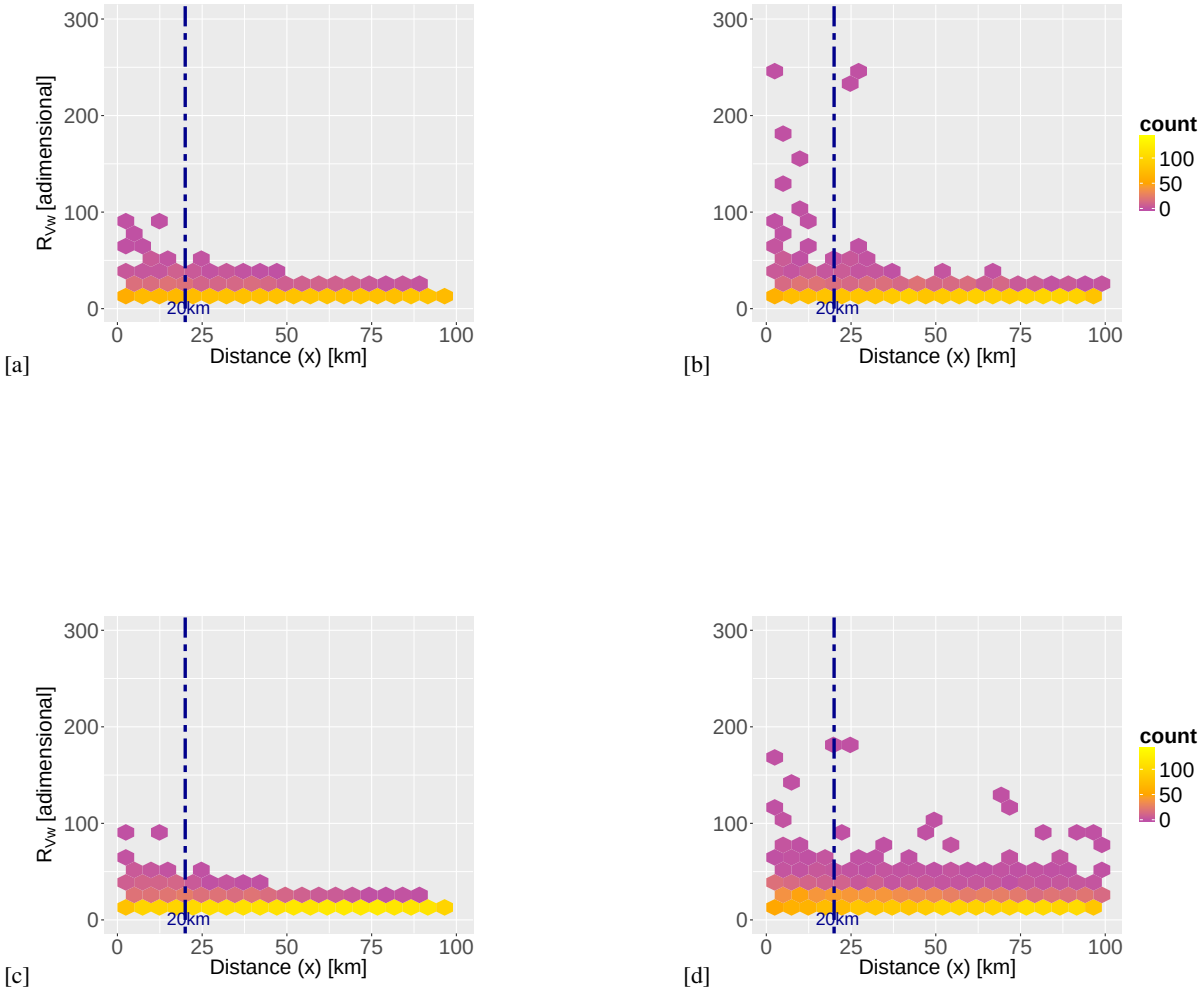

Figure 6. Heatmap of the anisotropy ratio of the wind velocity (R_{V_w}) against distance to the coast for a) south control transect (near the Ebre delta), b) central-south transect (near Tarragona harbour), c) central-north transect (near Mataro harbour) and d) north control transect (near Begur cape). All plots correspond to February 2017.

Ocean Sci. Discuss., https://doi.org/10.5194/os-2018-83
Manuscript under review for journal Ocean Sci.
Discussion started: 6 September 2018

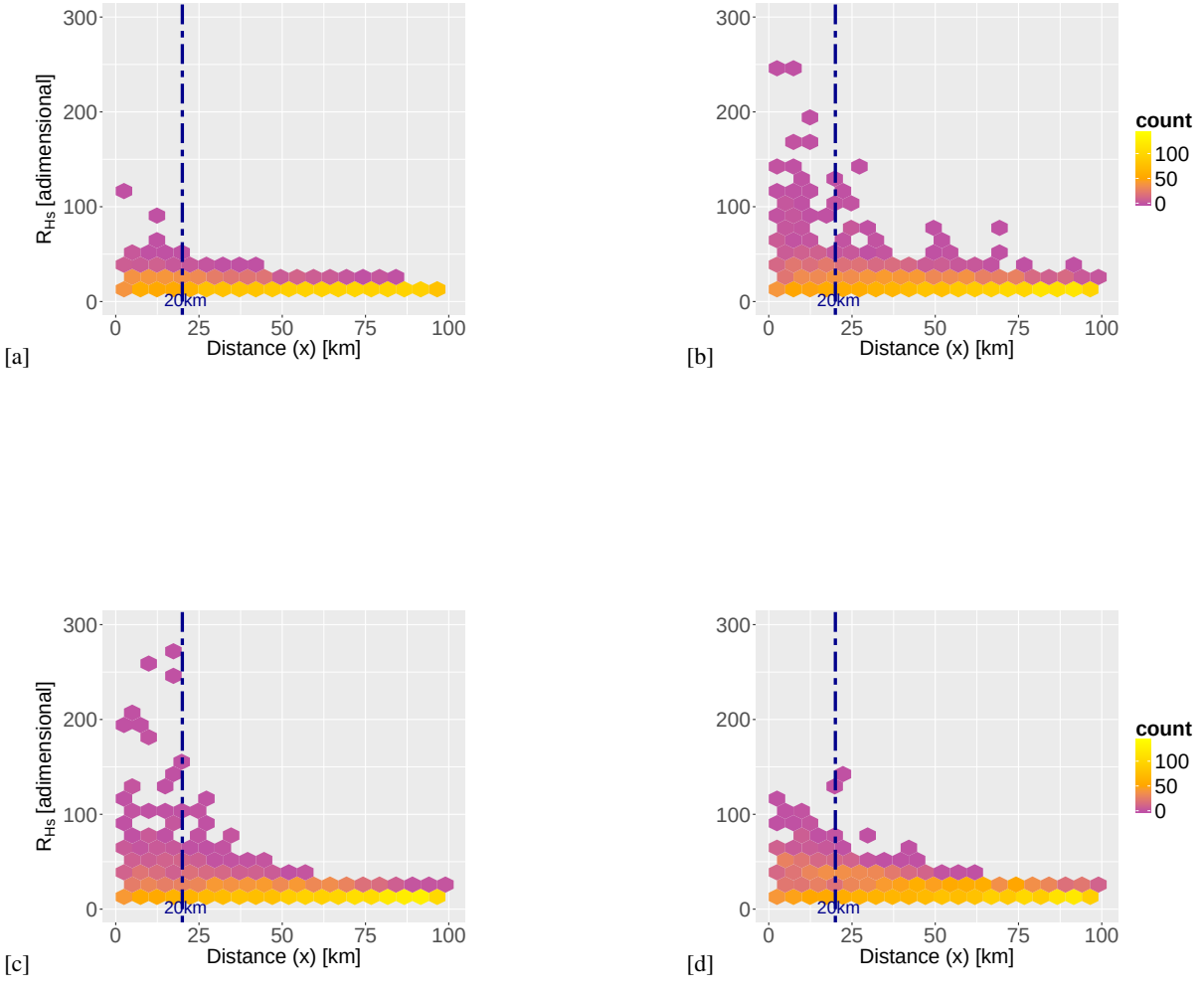

Figure 7. Heatmap of anisotropy ratio of significant wave height (R_{H_s}) against distance to the coast for a) south control transect (near the Ebre delta), b) central-south transect (near Tarragona harbour), c) central-north transect (near Mataro harbour) and d) north control transect (near Begur cape). All plots correspond to February 2017.

Ocean Sci. Discuss., https://doi.org/10.5194/os-2018-83
Manuscript under review for journal Ocean Sci.
Discussion started: 6 September 2018

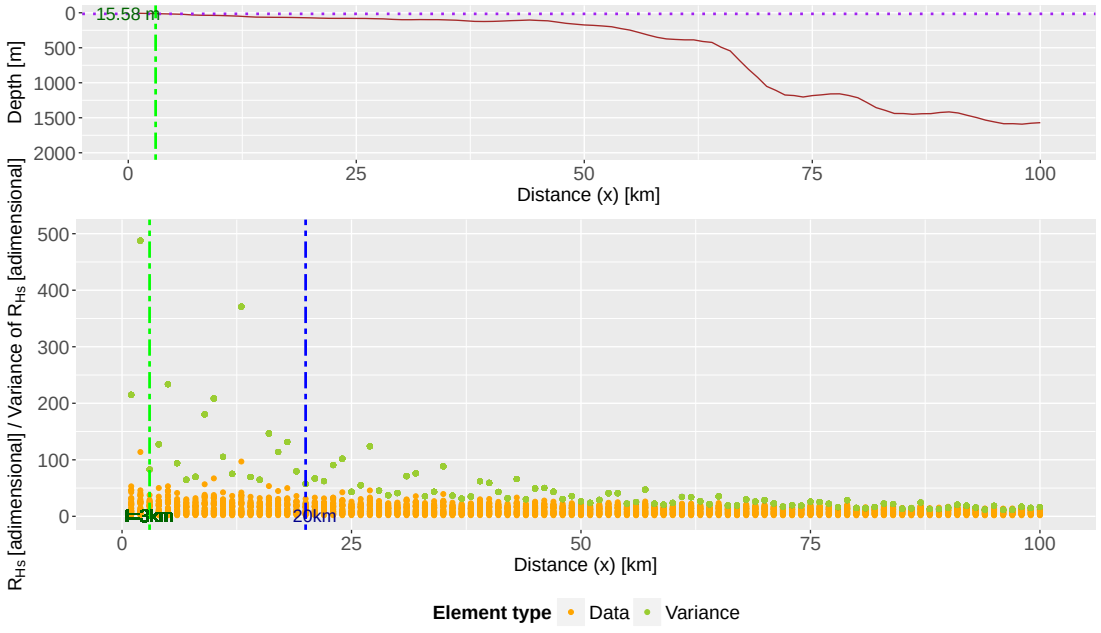

[a]

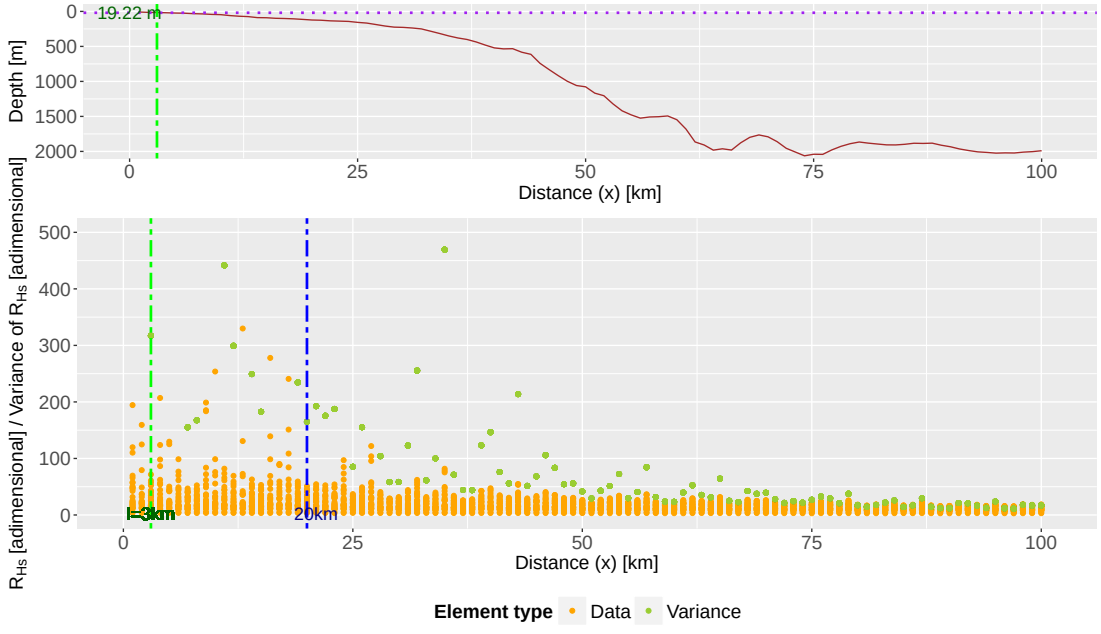

[b]

Figure 8. Relation for winter conditions (February 2017) between distance to the coast x, depth (upper plot) and anisotropy ratio of significant wave height (R_{H_s}), from shore to 100km offshore. Locations are a) south control transect (near the Ebre delta) and b) central-north transect (near Mataro harbour). The distance of 20km which has been suggested as a rough order of magnitude limit for direct applicability of Sentinel data is also shown (blue dashed line) together with the variance of R_{H_s} across the transect. From here, the coastal zone anisotropy-based boundary has been calculated and is also depicted. A green dash-dot line delimits its horizontal distance from the coast, whereas a purple dotted line denotes its elevation.

Ocean Sci. Discuss., https://doi.org/10.5194/os-2018-83
Manuscript under review for journal Ocean Sci.
Discussion started: 6 September 2018

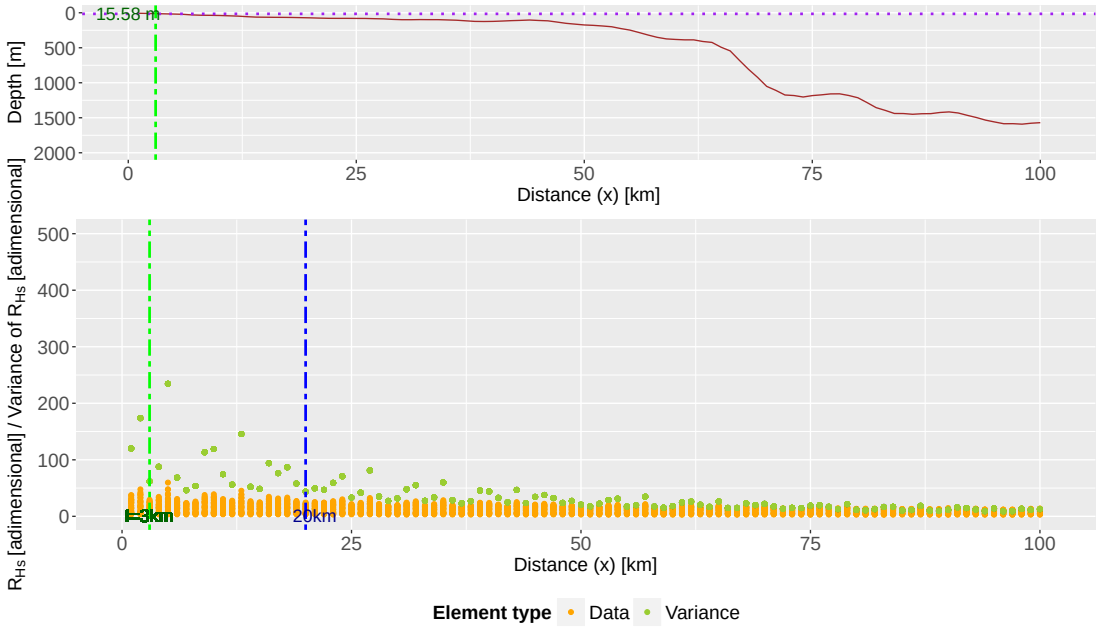

[a]

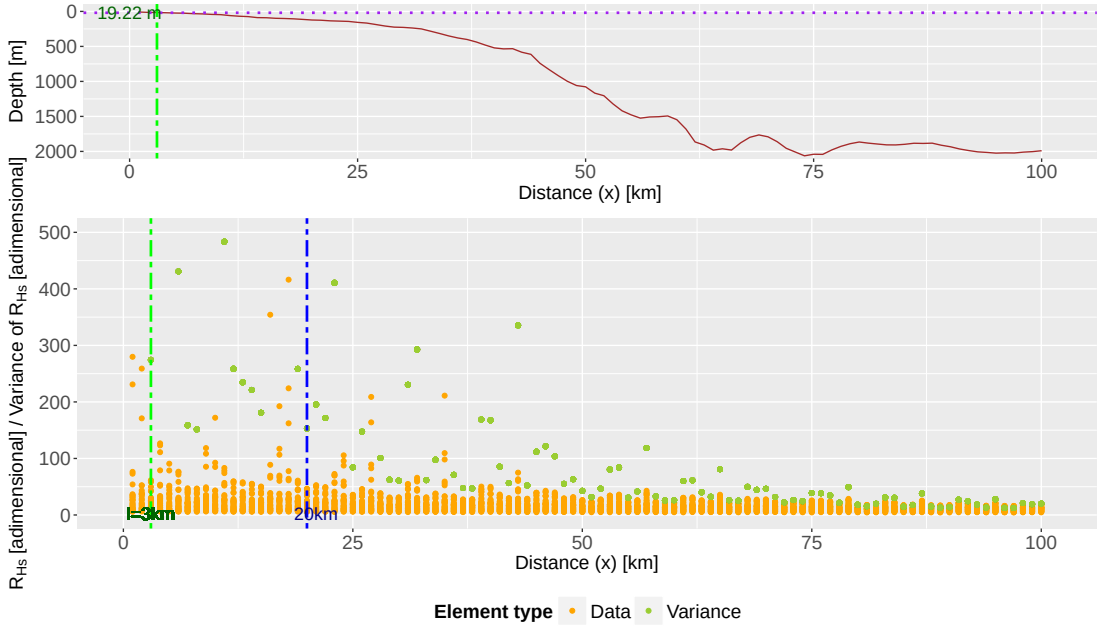

[b]

Figure 9. Relation for end of summer conditions (November 2016) between distance to the coast x, depth (upper plot) and anisotropy ratio of significant wave height (R_{H_s}), from shore to 100km offshore. Locations are a) south control transect (near the Ebre delta) and b) central-north transect (near Mataro harbour). The distance of 20km which has been suggested as a rough order of magnitude limit for direct applicability of Sentinel data is also shown (blue dashed line) together with the variance of R_{H_s} across the transect. From here, the coastal zone anisotropy-based boundary has been calculated and is also depicted. A green dash-dot line delimits its horizontal distance from the coast, whereas a purple dotted line denotes its elevation.

Ocean Sci. Discuss., https://doi.org/10.5194/os-2018-83
Manuscript under review for journal Ocean Sci.
Discussion started: 6 September 2018

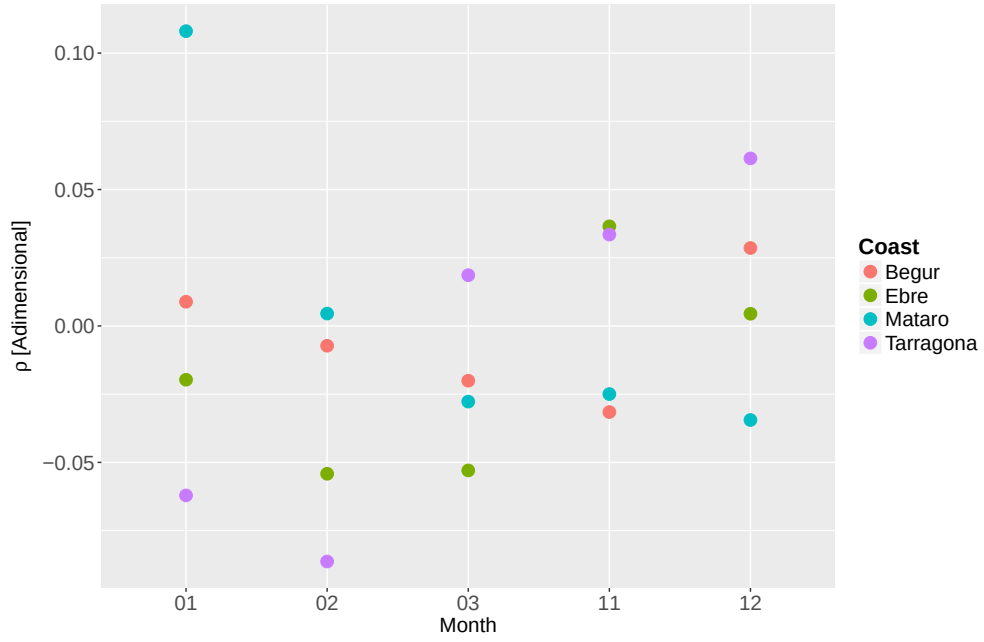

Figure 10. Copula parameters ρ of the proposed Gaussian copulas for all considered profiles: a) south control transect (near the Ebre delta), b) central-south transect (near Tarragona harbour), c) central-north transect (near Mataro harbour) and d) north control transect (near Begur cape). The plot shows the variation with time (horizontal axis) for five different months within a year cycle.

Higher values of R_{V_w} at distances from the coast below $20\mathrm{km}$ (see Fig. 6) indicate a clear directional spread of winds within the coastal fringe, linked to orographic control such as channelling by local mountains and river valleys.

The numerical wind fields present errors below $2\mathrm{m/s}$ (Martin et al., 2006), which means that the V_w calculated can represent well actual wind conditions. The behaviour of R_{V_w} near the coast can, nevertheless show sharp local variations due to the joint effect of orography, mesoscale circulation and large-scale circulation, all affecting wind strength and directionality. In all cases V_w becomes more isotropic towards the offshore, denoting a decreasing control by the land-water boundary.

The R_{H_s} pattern is similar, with wave fields showing boundary effects (mainly in directional properties) for coastal distances below 50km, which has also been considered an order of magnitude estimate for land wind effects. Farther from the coast there is a clear trend to isotropy, more pronounced for transects with more stable atmospheric conditions. The link between R_{H_s} and land-originated winds can be appreciated by the shift from homogeneous to anisotropic behaviour in the northern most transect (Begur) where the effect of V_w on H_s is only evident up to $38\mathrm{km}$ from the coast.

Such behaviour of R_{H_s} with coastal distance parallels that of particulate matter diffusivity, which tends to become isotropic at around $10\mathrm{km}$ (Romero et al., 2013) from the land-water boundary. The degree of anisotropy in diffusivity is physically related to eddy kinetic energy, which varies as $x^{5/4}$ (x being separation distance) for depths below $20\mathrm{m}$ (Gràcia et al., 1999). A steep bottom slope will favour deep-water wave behaviour at relatively short distances from the coast, as shown by the distinctive behaviour of R_{H_s} for coasts of different slope. However, although R_{H_s} presents greater variance (more outliers)

Ocean Sci. Discuss., https://doi.org/10.5194/os-2018-83
Manuscript under review for journal Ocean Sci.
Discussion started: 6 September 2018

for steep slopes (e.g. the due to the combination of deep and shallow water wave regimes as in the central-north transect, near Mataro harbour) the gradient of R_{H_s} with distance to the coast is similar for all types of bathymetry considered, suggesting a generic value of the proposed approach.

The ρ parameter of the Gaussian copula, characterizing the dependence structure among R_{V_w} and R_{H_s} reflects a certain similarity of the spatial behaviour for both variables, R_{V_w} and R_{H_s} (see Figs. 6 and 7). The mutual dependence of R_{V_w} and R_{H_s} is strongest for the northern-most transect (Begur), where the topo-bathymetric control of the Pyrenees and their submerged signature becomes better defined. Such mutual dependence gets weaker for the central and southern coastal transects (see Fig. 10). There seems to be a strong wind channelling aligned with the main river valleys (Sánchez-arcilla et al., 2014) in February and March, dominating the local wave fields. The ρ parameter should reflect this spatial and temporal variation, resulting in a coastal zone width that will be a function of the prevailing met-ocean drivers and should thus be considered as a dynamic concept. The resulting coastal definition will be data (numerical or observed) driven, being directly applicable to any region with a forecasting system or with enough coverage of in-situ plus satellite data. The proposed criteria appear to work well for wave-dominated and micro-tidal environments, and although suitable for any combination of factors, their application to macro-tidal regimes or river-discharge dominated areas should account for the corresponding signature in the hydrodynamic fields. Under these conditions the preferred variable could change to current velocity or to temperature, considering in all cases the effect of spatial resolution in the results.

7 Conclusions

The proposed coastal fringe (water sub-domain) definition is based on an objective estimation of anisotropy as a proxy for the influence of the land border. The suggested statistical assessment can be applied to any variable that reflects such an influence (here it has been illustrated with wind velocity and significant wave height) and can be easily automated for any field, numerical or observational, that presents enough resolution.

The methodology has been tested with numerically generated fields, supported by datasets from Puertos del Estado buoys. Anisotropies of wind velocity and significant wave heights have been extracted along a set of characteristic profiles spanning widths up to $100\mathrm{km}$ (see Fig. 2), considered sufficient for the relatively narrow shelfs in the Spanish Mediterranean coast. The performed analysis has shown how wind and wave fields are influenced by the land-sea border, demonstrating the topo-bathymetric control on met-ocean factors. This control depends on topographic (mountain chains and river valleys) and bathymetric (bottom slope, submarine canyons or prodeltas) features but also on the energetic level of the prevailing weather, leading to a dynamic definition of the coastal water domain. The resulting widths, based on variance variation, span distances in the kilometre range, depending on bottom slope and coastal plan shape geometry. The correlation between the wind and wave based definitions (i.e. the mutual dependence among R_{V_w} and R_{H_s}) seems to be stronger in the northern-most parts of the study area, where the topo-bathymetric control is most prominent.

This new definition of the coastal zone can be useful for setting up standards to delimitate this transitional fringe, facilitating the selection of processes and boundary conditions for modelling and providing an objective limit for impact assessments.

Ocean Sci. Discuss., https://doi.org/10.5194/os-2018-83
Manuscript under review for journal Ocean Sci.
Discussion started: 6 September 2018

Such an approach can also support directional and asymmetric measures of error and the underlying metrics (between model and data), leading to improved products and standards in the coastal zone.

Acknowledgements. This paper has been supported by the European project CEASELESS (H2020-730030-CEASELESS) and the Spanish national projects COBALTO (CTM2017-88036-R) and ECOSISTEMA-BC (CTM2017-84275-R). As a group, we would like to thank the Secretary of Universities and Research of the department of Economics of the Catalan Generalitat (Ref. 2014SGR1253). We duly thank the Meteorological Office of the United Kingdom for the provided wind fields and Puertos del Estado for the wave observations.

Ocean Sci. Discuss., https://doi.org/10.5194/os-2018-83
Manuscript under review for journal Ocean Sci.
Discussion started: 6 September 2018

References

Abdalla, S., Janssen, P. A. E. M., and Bidlot, J.: On the accuracy of surface wind and wind-wave data, in: Proceedings of the 10th International Conference on the Mediterranean Coastal Environment, MEDCOAST 11, pp. 25–29, 2011.

Ahsbahs, T., Badger, M., Karagali, I., and Larsén, X.: Validation of Sentinel-1A SAR Coastal Wind Speeds Against Scanning LiDAR, Remote Sensing, 9, 552, 2017.

Aitchison, J. and Brown, J. A. C.: The lognormal distribution with special reference to its uses in economics, 1957.

Amadei, B.: Importance of anisotropy when estimating and measuring in situ stresses in rock, in: International Journal of Rock Mechanics and Mining Sciences & Geomechanics Abstracts, vol. 33, pp. 293–325, Elsevier, 1996.

Bolaños, R. and Sánchez-Arcilla, A.: A note on nearshore wave features: Implications for wave generation, Progress in Oceanography, 70, 168–180, 2006.

Bolaños, R., Sánchez-Arcilla, A., and Cateura, J.: Evaluation of two atmospheric models for wind-wave modelling in the NW Mediterranean, Journal of Marine Systems, 65, 336–353, 2007.

Bolaños, R., Jorda, G., Cateura, J., Lopez, J., Puigdefabregas, J., Gomez, J., and Espino, M.: The XIOM: 20 years of a regional coastal observatory in the Spanish Catalan coast, Journal of Marine Systems, 77, 237–260, 2009.

Booij, N., Ris, R., and Holthuijsen, L.: A third-generation wave model for coastal regions, Part I, Model description and validation, Journal of Geophysical Research, 104 (C4), 7649–7666, 1999.

Brown, A., Milton, S., Cullen, M., Golding, B., Mitchell, J., and Shelly, A.: Unified modeling and prediction of weather and climate: A 25-year journey, Bulletin of the American Meteorological Society, 93, 1865–1877, 2012.

Carniel, S., Wolf, J., Brando, V. E., and Kantha, L. H.: Preface: Oceanographic processes on the continental shelf: observations and modeling, Ocean Science, 13, 495, 2017.

Casas-Prat, M. and Sierra, J.: Projected Future Wave Climate in the NW Mediterranean Sea, Journal of Geophysical Research: Oceans, 118, 3548–3568, 2013.

Cavaleri, L. and Sclavo, M.: The calibration of wind and wave model data in the Mediterranean Sea, Coastal Engineering, 53, 613 – 627, 2006.

Cerralbo, P., Grifoll, M., Moré, J., Bravo, M., Sairouní, A., and Espino, M.: Wind variability in a coastal area (Alfacs Bay, Ebro River delta), Advances in Science and Research, 12, 11–21, 2015.

Chen, C.-S., Liu, H.-D., and Beardsley, R. C.: An unstructured grid, finite-volume, three-dimensional, primitive equations ocean model: Application to coastal ocean and estuaries, Journal of atmospheric and oceanic technology, 20, 159–186, 2003.

Chorti, A. and Hristopulos, D. T.: Nonparametric identification of anisotropic (elliptic) correlations in spatially distributed data sets, IEEE Transactions on signal processing, 56, 4738–4751, 2008.

Crampin, S.: An introduction to wave propagation in anisotropic media, Geophysical Journal International, 76, 17–28, 1984.

Cullen, M. J. P.: The unified forecast/climate model, Meteorological Magazine, 122, 81–94, 1993.

Embrechts, P., Lindskog, F., and McNeil, A.: Modelling dependence with copulas, Rapport technique, Département de mathématiques, Institut Fédéral de Technologie de Zurich, Zurich, 2001.

García, M., Sánchez-Arcilla, A., Sierra, J., Sospedra, J., and Gómez, J.: Wind waves off the Ebro Delta, NM Mediterranean, Marine Systems, 4, 235–262, 1993.

Gràcia, V., Jimenez, J. A., Sánchez-Arcilla, A., Guillén, J., and Palanques, A.: Short-term relatively deep sedimentation on the Ebro delta coast. Opening the closure depth, in: Coastal Engineering 1998, pp. 2902–2912, 1999.

IPCC: Summary for policymakers. Emissions Scenarios. A Special Report of Working Group III of the Intergovernmental Panel of Climate Changefried, Tech. rep., IPCC, 2000.

Jones, J. E. and Davies, A. M.: Influence of non-linear effects upon surge elevations along the west coast of Britain, Ocean Dynamics, 57, 401–416, 2007.

Jordi, A., Basterretxea, G., and Wang, D.-P.: Local versus remote wind effects on the coastal circulation of a microtidal bay in the Mediterranean Sea, Journal of Marine Systems, 88, 312–322, 2011.

Lebeaupin Brossier, C., Béranger, K., and Drobinski, P.: Ocean response to strong precipitation events in the Gulf of Lions (northwestern Mediterranean Sea): A sensitivity study, Ocean Dynamics, 62, 213–226, 2012.

Lermusiaux, P. F., J., Schröter, J., Danilov, S., Iskandarani, M., Pinardi, N., and Westerink, J. J.: Multiscale modeling of coastal, shelf, and global ocean dynamics, Ocean Dynamics, 63, 1341–1344, 2013.

Li, F., van Gelder, P., Vrijling, J., Callaghan, D., Jongejan, R., and Ranasinghe, R.: Probabilistic estimation of coastal dune erosion and recession by statistical simulation of storm events, Applied Ocean Research, 47, 53 – 62, 2014.

Lin-Ye, J., Garcia-Leon, M., Gracia, V., and Sanchez-Arcilla, A.: A multivariate statistical model of extreme events: An application to the Catalan coast, Coastal Engineering, 117, 138 – 156, 2016.

Lin-Ye, J., García-León, M., Gràcia, V., Ortego, M. I., Lionello, P., and Sánchez-Arcilla, A.: Multivariate statistical modelling of future marine storms, Applied Ocean Research, 65, 192–205, 2017.

Martin, G. M., Ringer, M. A., Pope, V. D., Jones, A., Dearden, C., and Hinton, T. J.: The physical properties of the atmosphere in the new Hadley Centre Global Environmental Model (HadGEM1). Part I: Model description and global climatology, Journal of Climate, 19, 1274–1301, 2006.

Nicolle, A., Garreau, P., and Liorzou, B.: Modelling for anchovy recruitment studies in the Gulf of Lions (Western Mediterranean Sea), Ocean Dynamics, 59, 953–968, 2009.

Obermann, A., Bastin, S., Belamari, S., Conte, D., Gaertner, M. A., Li, L., and Ahrens, B.: Mistral and Tramontane wind speed and wind direction patterns in regional climate simulations, Climate Dynamics, pp. 1–18, 2016.

Obermann-Hellhund, A., Conte, D., Somot, S., Torma, C. Z., and Ahrens, B.: Mistral and Tramontane wind systems in climate simulations from 1950 to 2100, Climate Dynamics, pp. 1–11, 2017.

Okhrin, O., Okhrin, Y., and Schmid, W.: Properties of hierarchical Archimedean copulas, in: Statistics and Risk Modeling, 2013.

Pallarés, E.: High-resolution wave forecasting: the Catalan coast case: modelling, coupling and validation, Ph.D. thesis, 2016.

Pallarés, E., Espino, M., and Sánchez-Arcilla, A.: The relevance of the whitecapping term in wave forecasting. An analysis for the wave period of the Catalan coast., in: EGU General Assembly Conference Abstracts, vol. 15, p. 7867, 2013.

Pallarés, E., Sánchez-Arcilla, A., and Espino, M.: Wave energy balance in wave models (SWAN) for semi-enclosed domains–appication to the Catalan coast, Continental Shelf Research, 87, 41–53, 2014.

Pallarés, E., López, J., Espino, M., and Sánchez-Arcilla, A.: Comparison between nested grids and unstructured grids for a high-resolution wave forecasting system in the western Mediterranean sea, Journal of Operational Oceanography, 10, 45–58, 2017.

Roland, A. and Ardhuin, F.: On the developments of spectral wave models: Numerics and parameterizations for the coastal ocean, Ocean Dynamics, 64, 833–846, 2014.

Romero, L., Uchiyama, Y., Ohlmann, J. C., McWilliams, J. C., and Siegel, D. A.: Simulations of nearshore particle-pair dispersion in Southern California, Journal of Physical Oceanography, 43, 1862–1879, 2013.

Rueda, A., Camus, P., Tom A., Vitousek, S., and Mez, F.: A multivariate extreme wave and storm surge climate emulator based on weather patterns, Ocean Modelling, 104, 242 – 251, https://doi.org/http://dx.doi.org/10.1016/j.ocemod.2016.06.008, 2016.

Sánchez-Arcilla, A. and Simpson, J. H.: The narrow shelf concept: couplings and fluxes, Continental Shelf Research, 22, 153 – 172, https://doi.org/https://doi.org/10.1016/S0278-4343(01)00052-8, fluxes Across a Narrow Shelf, 2002.

Sánchez-Arcilla, A., Gónzalez-Marco, D., and Bolaños, R.: A review of wave climate and prediction along the Spanish Mediterranean coast, Nat. Hazard. Earth Sys., 8(6), 1217–1228, 2008.

Sánchez-Arcilla, A., García, M., and Gràcia, V.: Hydro-morphodynamic modelling in Mediterranean storms - errors and uncertainties under sharp gradients, Nat. Hazards Earth Syst. Sci., 14, 2993–3004, https://doi.org/10.5194/nhess-14-2993-2014, 2014.

Sánchez-arcilla, A., García-León, M., and Gràcia, V.: Hydro morphodynamic modelling in Mediterranean storms: errors and uncertainties under sharp gradients, Natural hazards and earth system sciences, 2, 1693–1728, 2014.

Sánchez-Arcilla, A., Gómez, M., Gràcia, V., Gironella, X., and García-León, M.: Reliability analysis of beaches as defenses against storm impacts under a climate change scenario, Coastal Engineering Proceedings, 1, 12, 2014.

Sánchez-Arcilla, A., García-León, M., Gràcia, V., Devoy, R., Stanica, A., and Gault, J.: Managing coastal environments under climate change: pathways to adaptation, Science of the Total Environment, 572, 1336–1352, 2016a.

Sánchez-Arcilla, A., Sierra, J. P., Brown, S., Casas-Prat, M., Nicholls, R. J., Lionello, P., and Conte, D.: A review of potential physical impacts on harbours in the Mediterranean Sea under climate change, Regional Environmental Change, pp. 1–14, 2016b.

Sánchez-Arcilla, A., Carniel, S., Badger, M., Bidlot, J., Hansen, L. B., Bolaños-Sánchez, R., Cipollini, P., Espino, M., Miglietta, M. M., Saulter, A., and Staneva, J.: The challenges of coastal oceanography. Prediction limits and new applications based on Sentinel data, in: EGU General Assembly Conference Abstracts, vol. 19, p. 14638, 2017.

Schaeffer, A., Molcard, A., Forget, P., Fraunié, P., and Garreau, P.: Generation mechanisms for mesoscale eddies in the Gulf of Lions: Radar observation and modeling, Ocean Dynamics, 61, 1587–1609, 2011.

Sierra, J. P., García-León, M., Gràcia, V., and Sánchez-Arcilla, A.: Green measures for Mediterranean harbours under a changing climate, in: Proceedings of the Institution of Civil Engineers-Maritime Engineering, pp. 1–12, Thomas Telford Ltd, 2017.

Sklar, A.: Fonctions dé repartition à n dimension et leurs marges, Université Paris 8, 1959.

Soomere, T.: Anisotropy of wind and wave regimes in the Baltic Proper, Journal of Sea Research, 49, 305–316, 2003.

Swail, V., Komen, G., Ryabinin, V., Holt, M., Taylor, P. K., and Bidlot, J.: Wind waves in the Global Ocean Observing System, in: OCEANOBS99, Proc. of the Int. Conf on the Ocean Observing System for Climate, St. Raphael, France, 1999.

Verdon, J. P., Angus, D. A., Kendall, J. M., and Hall, S. A.: The effect of microstructure and nonlinear stress on anisotropic seismic velocities, Geophysics, 2008.

Wahl, T., Jensen, J., and Mudersbach, C.: A multivariate statistical model for advanced storm surge analyses in the North Sea, Coastal Engineering Proceedings, 1, 19, 2011.

Wright, L. D. and Short, A. D.: Morphodynamic variability of surf zones and beaches: A synthesis, Marine geology, 56, 93–118, 1984.

Zijlema, M.: Computation of wind-wave spectra in coastal waters with SWAN on unstructured grids, Coastal Engineering, 57, 267 – 277, https://doi.org/http://dx.doi.org/10.1016/j.coastaleng.2009.10.011, 2010.